Solidification of Two-Dimensional Viscous, Incompressible Stagnation Flow

Ali Shokrgozar Abbassi

Asghar B. Rahimi[1]
Professor
e-mail: rahimiab@yahoo.com

Faculty of Engineering,
Ferdowsi University of Mashhad,
P. O. Box No. 91775- 1111,
Mashhad, Iran

The history of the study of fluid solidification in stagnation flow is limited to a few cases. Among these few studies, only some articles have considered the fluid viscosity and yet pressure variations along the thickness of the viscous layer have not been taken into account and the energy equation has been assumed to be one-dimensional. In this study the solidification of stagnation flows is modeled as an accelerated flat plate moving toward an impinging fluid. The unsteady momentum equations, taking the pressure variations along viscous layer thickness into account, are reduced to ordinary differential equations by the use of proper similarity variables and are solved by using a fourth-order Runge-Kutta integrating method at each prescribed interval of time. In addition, the energy equation is numerically solved at any step for the known velocity and the problem is presented in a two-dimensional Cartesian coordinate. Comparisons of these solutions are made with existing special ranges of past solutions. The fluid temperature distribution, transient velocity component distribution, and, most important of all the rate of solidification or the solidification front are presented for different values of nondimensional Prandtl and Stefan numbers. The results show that an increase of the Prandtl numbers (up to ten times) or an increase of the heat diffusivity ratios (up to two times) causes a decrease of the ultimate frozen thickness by almost half, while the Stefan number has no effect on this thickness and its effect is only on the freezing time.
[DOI: 10.1115/1.4023936]

Keywords: solidification, viscous incompressible fluid, exact solution, stagnation flow, unsteady

1 Introduction

The solidification that comprises the heat transfer accompaniment phase change is one of the most interesting phenomena in natural processes and industrial applications. The glass, metal, plastic, oil industries, food-providing, and other corresponding industries need a good understanding of solidification behavior and the nature of solid growth.

In addition, studies of the phase change in stagnant media and better understanding of the convection effect upon the interface behavior and solidification properties are needed to meet industrial demands, such as the desire for more homogenous semiconductor crystals in the nuclear industry, along with the better understanding of natural ice formation.

The classic problem of stagnant fluid solidifying on a cold plate has been solved by Stefan [1]. A one dimensional heat flux method for the phase change problem has been presented by Goodrich [2]. This method is accompanied by simplifications such as the assumption of one dimensionality of the solid-liquid interface. Experiments were performed in order to study the transition between freezing controlled by natural convection in the liquid adjacent to a freezing interface and freezing controlled by heat conduction in the solidified material by Sparrow [3]. Additionally, a numerical method for solidifying in natural convection is used by Lacroix [4] and the three-dimensional problem for natural convection with the accompaniment of the phase change in a rectangular channel is solved by Yeoh et al. [5], in which the fluid properties vary with temperature. The solidification of a fluid layer confined between two isolated plates is investigated by Hadji et al. [6]. Another method for calculating the heat flux, depending on time in natural convection, is presented by Hanumanth [7]. A combined model for the phase change upon various states of pure substances and the melting fluid problem due to spreading and solidifying on the flat plate and a numerical modeling of the forming and solidifying of a droplet on a cold plate is investigated in Refs. [8–10]. The evolution due to impact on the substrate plate and the solidifying of a droplet is presented by San Marchi et al. [11]. Concentrating upon the stagnation flow, the solidification of an inviscid fluid at an interface and the effect of its phenomena on morphological instability is investigated by Brattkus et al. [12]. The Stefan problem for inviscid stagnation flow by two methods and the solidifying of super-cooled liquid stagnation inviscid flow are considered by Rangel and Lambert [13,14], respectively, in which a numerical solution to the problem using an interface tracking method is compared to analytical solutions for the instantaneous similarity and quasi-steady state. Additionally, the solidification of a viscous stagnation flowwas investigated by Rangel and Bian [15] with the pressure consideration only along the flow and not along the boundary layer and by applying the method of instantaneous similarity, the temperature field, the solid-liquid interface location, and its growth rate that is valid for the initial stages of solidification were obtained. Furthermore, with the use of the quasi-state approximation a solution of the problem that is valid for the final stages of solidification is obtained. A power series solution of viscous stagnation has been presented by Yoo [16] in which the solution at the initial stage of freezing is obtained by expanding it in powers of time and the final equilibrium state is determined from the steady-state governing equations. Recently Shokrgazr Abbasi and Rahimi [17] have studied the stagnation-point flow and heat transfer impinging on an accelerated flat plate which can be used in the modeling of solidification in a general and unified manner. New research in the area of stagnation flow obtaining exact solutions can be found in the papers by Hong et al. [18], Alassar et al. [19], and Norouzi et al. [20].

[1]Corresponding author.

Contributed by the Heat Transfer Division of ASME for publication in the Journal of Heat Transfer. Manuscript received July 2, 2012; final manuscript received March 1, 2013; published online June 17, 2013. Assoc. Editor: Ali Ebadian.

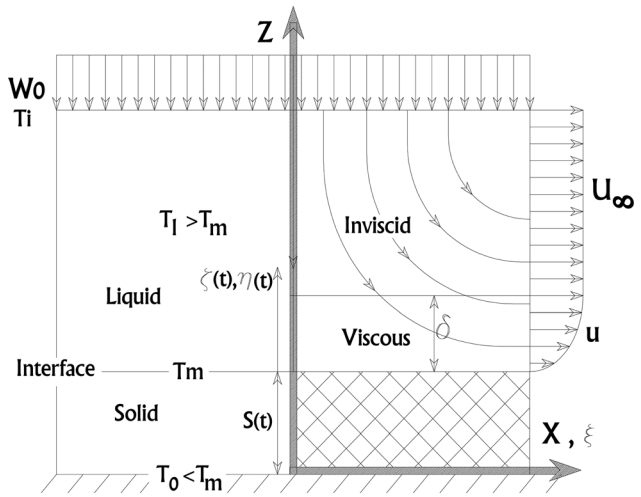

Fig. 1 Coordinate system

In this study the solidification of stagnation flows is modeled as an accelerated flat plate moving toward an impinging fluid, as in Ref. [17]. The unsteady momentum equations, taking into account the pressure variations along the viscous layer thickness, are reduced to ordinary differential equations bythe use of proper similarity variables and are solved by using a fourth-order Runge-Kutta integrating method at any prescribed interval of time. In addition, the energy equation upon the liquid phase, solid-liquid interface, and solid phase is solved by the finite difference method at any step for a known velocity and the problem is presented in two-dimensional Cartesian coordinates. Comparisons of these solutions are made with existing special ranges of past solutions. The fluid temperature distribution, transient velocity components distribution, and, most important of all, the rate of solidification or the solidification front are presented for different values of nondimensional Prandtl and Stefan numbers.

2 Problem Formulation

Figures 1 and 2 represent a two-dimensional Cartesian coordinate system (x, z) with corresponding (u, w) components of velocity. The viscous laminar unsteady incompressible stagnation flow with a strain rate $a(t)$ in the z-direction approaches to $z = 0$ perpendicular to the plate at $t = 0$. The fluid is solidified with variable solidification velocity and acceleration $\dot{S}(t)$ and $\ddot{S}(t)$, respectively, such as an imaginary plate at the solid-liquid interface with a moving distance of $S(t)$ towards the fluid in each time step. In

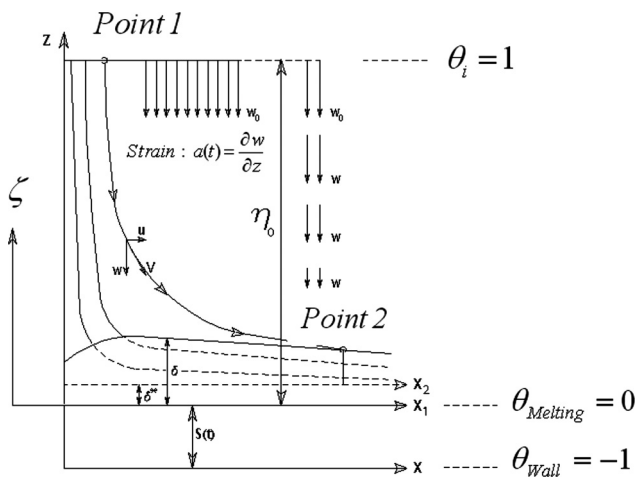

Fig. 2 Explanation of strain and stream lines

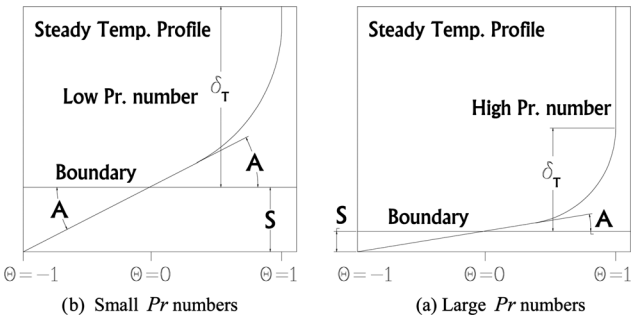

Fig. 3 Ultimate solidification thickness after stability of the thermal boundary layer for various Pr numbers and $\alpha_r = 1$

later sections we will see why this plate is considered as a flat one. Variation of the strain of the impinging fluid due to the moving solidification front is shown in Figure (3), as was shown in Ref. [17]. Note that a_0 is the strain at far field. The Navier–Stokes and energy equations in the unsteady state are

mass

$$\frac{\partial u}{\partial x} + \frac{\partial w}{\partial z} = 0 \tag{1}$$

momentum

$$\frac{\partial u}{\partial t} + u\frac{\partial u}{\partial x} + w\frac{\partial u}{\partial z} = -\frac{1}{\rho}\frac{\partial p}{\partial x} + \nu\left(\frac{\partial^2 u}{\partial x^2} + \frac{\partial^2 u}{\partial z^2}\right) \tag{2}$$

$$\frac{\partial w}{\partial t} + u\frac{\partial w}{\partial x} + w\frac{\partial w}{\partial z} = -\frac{1}{\rho}\frac{\partial p}{\partial z} + \nu\left(\frac{\partial^2 w}{\partial x^2} + \frac{\partial^2 w}{\partial z^2}\right) \tag{3}$$

energy

(a) in the liquid phase

$$\frac{\partial T}{\partial t} + u\frac{\partial T}{\partial x} + w\frac{\partial T}{\partial z} = \alpha_l\left(\frac{\partial^2 T}{\partial x^2} + \frac{\partial^2 T}{\partial z^2}\right) \tag{4}$$

(b) in the solid phase

$$\frac{\partial T}{\partial t} = \alpha_s\left(\frac{\partial^2 T}{\partial x^2} + \frac{\partial^2 T}{\partial z^2}\right) \tag{5}$$

(c) at the interface

$$\rho h_{ls}\frac{dS(t)}{dt} = k_s\frac{\partial T_s}{\partial z} - k_l\frac{\partial T_l}{\partial z} \tag{6}$$

in which p, ρ, ν, k, and α are the pressure, density, kinetic viscosity, conduction heat transfer coefficient, and thermal diffusivity, respectively, and dissipation is ignored because of the small velocities. The subscripts s and l denote the solid and liquid phases, respectively.

3 Solution

3.1 Fluid Flow Similarity Solution. According to Ref. [17], the velocity components in the viscous region are

$$u = a(t)xf'(\eta) \quad w(t) = -\sqrt{\frac{\nu}{a_\circ}}a(t)f(\eta)$$

$$\eta(t) = \sqrt{\frac{a_\circ}{\nu}}(z - S(t)) \quad \text{and} \quad \zeta(t) = z - S(t) \tag{7}$$

In which the terms involving $f(\eta)$ comprise the Cartesian similarity form for unsteady stagnation-point flow and the prime denotes differentiation with respect to η. Transformations (7) automatically satisfy Eq. (1) and their insertion into Eqs. (2) and (3) yields the following ordinary differential equation in terms of $f(\eta)$:

$$f''' + f''\left(\tilde{\dot{S}}(t) + \tilde{a}(t)f\right) - \tilde{a}(t)f'^2 - \frac{f'}{\tilde{a}(t)}\frac{d\tilde{a}(t)}{d\tau} + \frac{1}{\tilde{a}(t)\xi}\frac{\partial \tilde{P}}{\partial \xi} = \circ \quad (8)$$

in which

$$\frac{1}{\tilde{a}(t)\xi}\frac{\partial \tilde{p}}{\partial \xi} = -\tilde{a}(t) - \left(\frac{1}{\tilde{a}(t)}\frac{d\tilde{a}(t)}{d\tau} - \frac{2\eta\tilde{\dot{S}}}{\xi^2+\eta^2} + \frac{\tilde{\dot{S}}}{\eta}\right)\left(1 - \frac{\eta^2}{\xi^2}\right) \quad (9)$$

$$\frac{d\tilde{a}(t)}{d\tau} = \frac{-\tilde{a}_\circ \tilde{\dot{S}}}{\eta_\circ^2} + \frac{\tilde{\ddot{S}}}{\eta_\circ} + \frac{\tilde{\dot{S}}^2}{\eta_\circ^2} \quad (10)$$

and an expression for the pressure

$$\begin{aligned}\tilde{P} = {} & -\tilde{a}(t)(f'-1) - \tilde{a}(t)\tilde{\dot{S}}(f - f(\eta=\delta)) + \tilde{a}^2(t)\frac{(f^2 - f^2(\eta=\delta))}{2} \\ & - \frac{d\tilde{a}(t)}{d\tau}\int_\eta^\delta f(\eta)d\eta - \frac{\tilde{a}^2(t)}{2}\left(\xi^2+\eta^2\right) - \left[\frac{d\tilde{a}(t)}{d\tau}\left(\frac{\xi^2+\eta^2}{2}\right)\right. \\ & \left. - 2\tilde{a}(t)\tilde{\dot{S}}\int_\infty^2 \frac{\eta\left(\xi^2-\eta^2\right)}{\xi\left(\xi^2+\eta^2\right)^2}d\xi + \tilde{a}(t)\tilde{\dot{S}}\left(\frac{\xi^2}{3\eta} + \eta\right)\right]_\infty^\delta \end{aligned} \quad (11)$$

where

$$\begin{aligned}\tilde{P}(x,z,t) = \frac{p(x,z,t)}{\rho a_\circ \nu}, \quad \tilde{S}(t) = \sqrt{\frac{a_\circ}{\nu}}S(t), \quad \tilde{a}(t) = \frac{a(t)}{a_\circ}, \\ \tilde{\dot{S}}(t) = \dot{S}(t)/\sqrt{a_\circ \nu}, \quad \xi = \sqrt{\frac{a_\circ}{\nu}}x, \quad \tau = \frac{t}{1/a_\circ}, \\ \tilde{x} = x\sqrt{a_\circ/\nu}, \quad \tilde{z} = z\sqrt{a_\circ/\nu}\end{aligned} \quad (12)$$

in which $\tilde{P}$, $\tilde{S}$, $\tilde{\dot{S}}$, and $\tilde{x}$ are corresponding nondimensional quantities and the dot denotes differentiation with respect to t. Relation (11), which represents pressure, is obtained by integrating Eq. (3) in the z-direction and by use of the potential flow solution as the boundary conditions. The boundary conditions for the differential Eq. (8) are

$$\begin{aligned}\eta = 0: \quad & f = 0,\ f' = 0 \\ \eta \to \infty: \quad & f' = 1\end{aligned} \quad (13)$$

3.2 Heat Transfer. Using the nondimensional temperature as in Ref. [17]

$$\theta = \frac{T(\eta) - T_\infty}{T_w - T_\infty} \quad (14)$$

and using nondimensional quantities for the time as τ, distance from the x axis as $\tilde{x}$, and distance from the z axis as $\tilde{z}$, Eqs. (4)–(6) become

for the liquid phase

$$\frac{\partial \theta_l}{\partial \tau} + \tilde{u}\frac{\partial \theta_l}{\partial \tilde{x}} + \tilde{w}\frac{\partial \theta_l}{\partial \tilde{z}} = \frac{1}{\mathrm{Pr}}\left(\frac{\partial^2 \theta_l}{\partial \tilde{x}^2} + \frac{\partial^2 \theta_l}{\partial \tilde{z}^2}\right) \quad (15)$$

for the solid phase

$$\frac{\partial \theta_s}{\partial \tau} = \frac{1}{\mathrm{Pr}}\left(\frac{\partial^2 \theta_s}{\partial \tilde{x}^2} + \frac{\partial^2 \theta_s}{\partial \tilde{z}^2}\right) \quad (16)$$

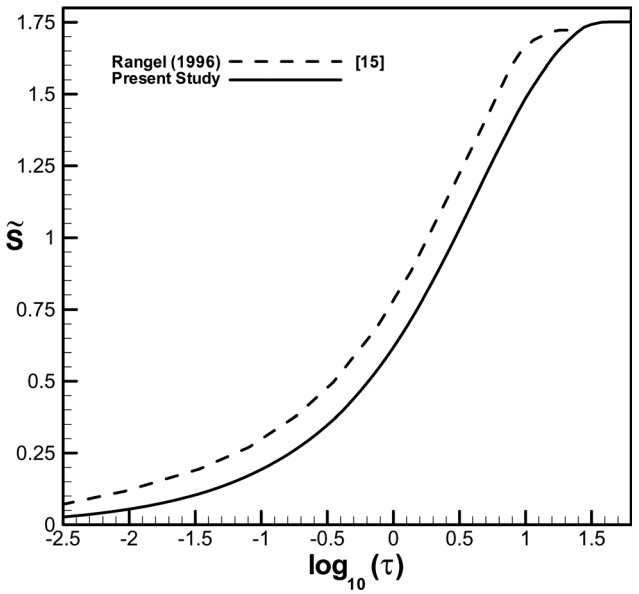

Fig. 4 Comparison of the present study and the Ref. [15] results for (Pr = 1, St = 1, $k_r = 1$, $\alpha_r = 1$ and $\theta_i = 1$)

and for the interface of the liquid and solid

$$\frac{a\mathrm{Pr}}{\mathrm{St}}\frac{d\tilde{S}}{d\tau} = \frac{\partial \theta_s}{\partial \tilde{z}} - b\frac{\partial \theta_l}{\partial \tilde{z}} \quad (17)$$

Equations (8)–(11) and (15)–(17), along with their boundary conditions, are solved in the next section.

4 Solution Method

First, the energy equation of the liquid-solid interface, Eq. (17), is numerically solved to find the freezing velocity $(d\tilde{S}/d\tau = \tilde{\dot{S}}(t))$, which is as unsteady term in Eq. (8). Thus, this equation is converted to an ordinary differential equation and is numerically solved using a shooting method trial and error based on the Runge-Kutta algorithm. The results for the velocity components are used in the energy Eq. (15) upon the liquid region to convert this nonlinear equation to a linear one. Then, this linear equation is discretized by using the power law scheme. For small Pe ($\mathrm{Pe} < 1$) and large Pe ($\mathrm{Pe} > 10$), this scheme is central and upwind, respectively, and for $1 < \mathrm{Pe} < 10$, the scheme is a combination of these two. To solve the produced algebraic system of equations, the TDMA[1] within the ADI[2] method is used.

5 Validation of the Results

In this section, our results are compared to previous studies. For the comparisons, Ref. [15] is the most complete and the best selection, since in this study fluid is viscous and a parametric study has been considered. The results of these two studies are presented together in Fig. 4 for $(\mathrm{Pr} = 1, \mathrm{St} = 1, \theta_i = 1, \alpha_r = 1,$ and $k_r = 1)$. As can be seen in this figure, due to the evolution of the frozen front, the average relative difference of the points is around 20%. This difference is expected, as in our study all effective parameters, such as the pressure variation along the boundary layer, are being taken into account.

6 Presentation of Results and Parametric Study

In this section, a parametric study is done for different values of $\mathrm{Pr}, \mathrm{St}, \theta_i, k_r,$ and α_r as the solidification is advancing. The

[1]Three diagonal matrix algorithm.
[2]Alternating direction implicit.

solidification front for $\mathrm{Pr}=10$ in our study has been compared with this quantity for $\mathrm{Pr}=100$ of Ref. [15] in Fig. 5. The reason for the selection of $\mathrm{Pr}=10$ is because the curve corresponding to $\mathrm{Pr}=100$ in our study would lie on the horizontal coordinate, although the following issues do not change. As can be seen from this figure, the direction of the variation of the solidification front with the Pr number in Ref. [15] is opposite from ours with the $\mathrm{Pr}=1$ base. This paradox leads us to look for a reliable method for finding the correct results, as discussed in the following text. One approach to find the correct answer is the use of an approximate analytical solution. The assumptions to obtain this analytical solution are as follows:

(1) The convection terms in the liquid-solid interface are negligible since the velocity is very low in this region.
(2) Conduction is one dimensional in the liquid-solid interface because of the previous assumptions. Here, the second assumption is, in fact, the result of the first one.

Note that the dimensionless temperature difference at the interface is zero, thus the energy equation in this region could be presented as

$$\Delta\tau = \frac{\mathrm{Pr}\cdot\Delta\tilde{z}^2}{\mathrm{St}}\frac{1}{\theta_l+\theta_s/\alpha_r} \tag{18}$$

where the upper and lower nodes in the fluid and solid regions are introduced by θ_l and θ_s, respectively. In this equation, the dimensionless time ($\Delta\tau$) tends to infinity as $(\theta_l+\theta_s/\alpha_r)\rightarrow 0$ and solidification is consequently stopped. Additionally, $\alpha_r=1$ is assumed for simplification. Figure 3 determines the ultimate solid thickness, which is equal to tan (A). It is determined from these figures that as the thickness of the temperature boundary layer increases, the ultimate solidification thickness increases and this increase is due to the decrease of the Pr number and vice versa. From this analytical approach, the ultimate solidification thickness for $\mathrm{Pr}=10$ must be smaller than the case of $\mathrm{Pr}=1$ and, therefore, the correct direction of variation of the solidification front in Fig. 5 would be the direction in our study. In adition, by taking just the effect of the Pr number into account, we see that an increase of this quantity increases the solidification time, as shown in Eq. (18). Therefore, the results of our study are validated, yet there is another simple approach to find the correct answer, which is shown in the following text.

The heat transfer rate upon the frozen region with constant k reads

$$q=-k\frac{\Delta T}{\Delta z} \tag{19}$$

where ΔT is the temperature difference between the liquid-solid interface and the substrate and, therefore, is a constant. The only way to increase the heat transfer rate is to decrease Δz, where Δz is the ultimate frozen thickness, which is same as in the steady-state case. Increasing the Pr number in the fluid region increases the Nusselt number and, consequently, increases the convection heat transfer coefficient (h) (see Ref. [21], pp. 134–135). By increasing this coefficient, heat transfer increases in the fluid region but the same heat rate must be taken out of the frozen region. Therefore, the ultimate solidification thickness decreases by increasing the Pr number. In fact, physically, increasing the Pr number increases heat transfer in the fluid region and this rapid heat transfer through the lower layers causes the fluid temperature to reach the freezing point at the interface and, consequently, the ultimate frozen thickness must decrease. Using the preceding discussion, we conclude that the results of Ref. [15] for $\mathrm{Pr}\neq 1$ are incorrect. The source of this incorrectness in Ref. [15] is the use of the wrong result from Eq. (22) in Eq. (23) of this reference. Equation (23) in Ref. [15] can produce curves with arbitrary trends for any particular Prandtl number since the choice of the upper limit of the integral in this equation is infinity and, therefore, in the numerical integration, different choices for this upper limit produce different curves. Therefore, the curve from Ref. [15] shown in Fig. 5 of our study can have an arbitrary trend, which is wrong.

In this section, the parametric study is continued without comparison with other studies. Variations of the solidification front are shown in Fig. 6 for $k_r=\alpha_r=0.5$ ($\mathrm{Pr}=1$, $\mathrm{St}=1$, and $\theta_i=1$). Since the k_r and α_r variations can also be special cases of the Pr variations, here the results of these two parameters are considered for a constant Pr number. Equation (18) shows that decreasing k_r and/or α_r by half increases the final solid thickness two times because the tan (a) increases two times; see Fig. 4. Additionally, since decreasing k_r and α_r causes a decrease of the rate of heat transfer in the liquid and solid, then at any particular location in the liquid the temperature is lower for the case of (k_r and α_r) <1, compared to the case of (k_r and α_r) $=1$ and, therefore, the former choice will increase the final thickness of the solid.

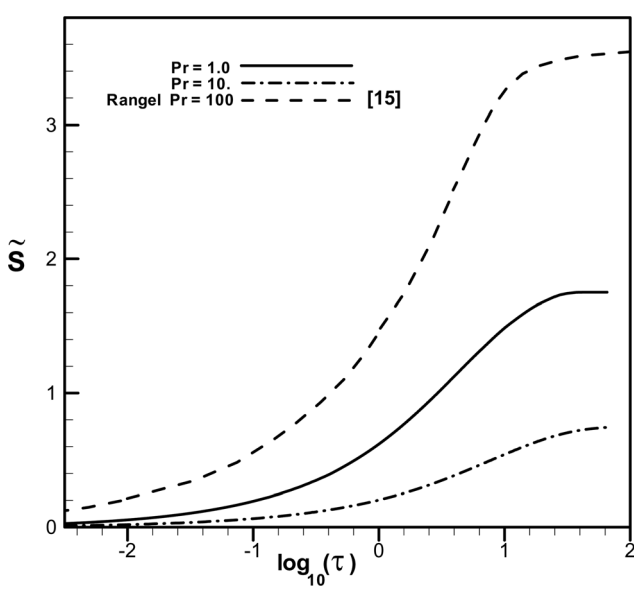

Fig. 5 Solidification front for $\mathrm{Pr}=10$ and ($\mathrm{St}=1$, $k_r=1$, $\alpha_r=1$, and $\theta_i=1$)

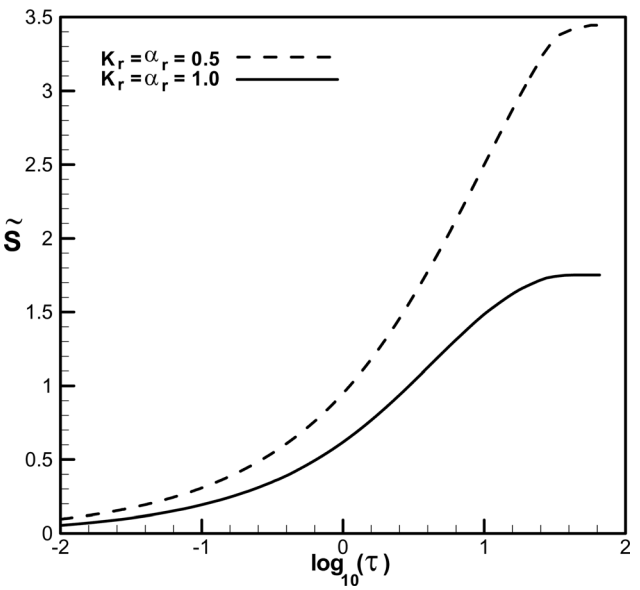

Fig. 6 Solidification front for $k_r=\alpha_r=0.5$ and ($\mathrm{Pr}=1$, $\mathrm{St}=1$, and $\theta_i=1$)

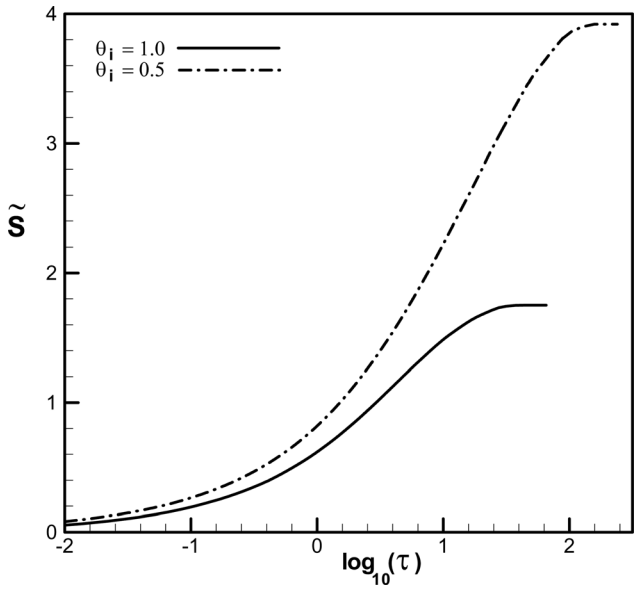

Fig. 7 Solidification front for $\theta_i = 0.5$ and (Pr = 1, St = 1, $k_r = 1$, and $\alpha_r = 1$)

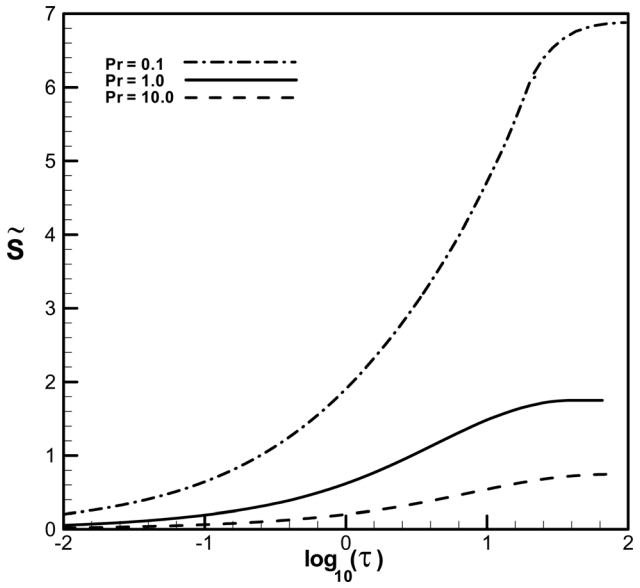

Fig. 9 Effect of the Pr number upon the solidification front for (St = 1, $k_r = 1$, $\alpha_r = 1$, and $\theta_i = 1$)

Figure (7) represents the frozen front results of this study for $\theta_i = 0.5$ (Pr$= 1, \mathrm{St} = 1, k_r = 1,$ and $\alpha_r = 1$). The variation of θ_i has interesting results. That is, at any particular location in the liquid the temperature is lower for the case of $\theta_i < 1$, compared to the case of $\theta_i = 1$. When θ_i tends to zero, the ultimate frozen thickness tends to infinity and this case requires a separate analysis.

Figure 8 represents the effect of the St number on the solidification front. By the use of Fig. 3 and Eq. (15) it is determined that the St number affects only the solidification time and has no effect on the final solid thickness. Figure 9 represents the effect of Pr number variations on the solidification front more completely. As previously mentioned, this figure shows that the increasing Pr number decreases the final solid thickness and vice versa. Additionally, Fig. 10 represents the increasing and decreasing k_r and/or α_r effects. As expected, Fig. 11 shows that increasing the initial liquid temperature difference decreases the thickness of the ultimate frozen thickness and vice versa.

Other interesting considerations are discussed in this section. At first, eliminating the effect of the temperature variation on the solidification time is considered. Figure 12 represents the results of this consideration for Pr $= 10$. More temperature differences between inlet and substrate temperatures leads to these two curves getting closer together and causes more error due to elimination. Table 1 gives the required time for the inlet liquid temperature reaching the freezing temperature versus the total time of the temperature variations and freezing ($\theta_i = 1$ and Pr$= 1, \mathrm{St} = 1,$ $k_r = 1,$ and $\alpha_r = 1$). This is 0.14 times the total time and, thus, it is not negligible.

Another interesting consideration is in the comparisons of the effect of the convection and conduction terms separately, as shown in Fig. 13. In fact, as previously mentioned, the effect of

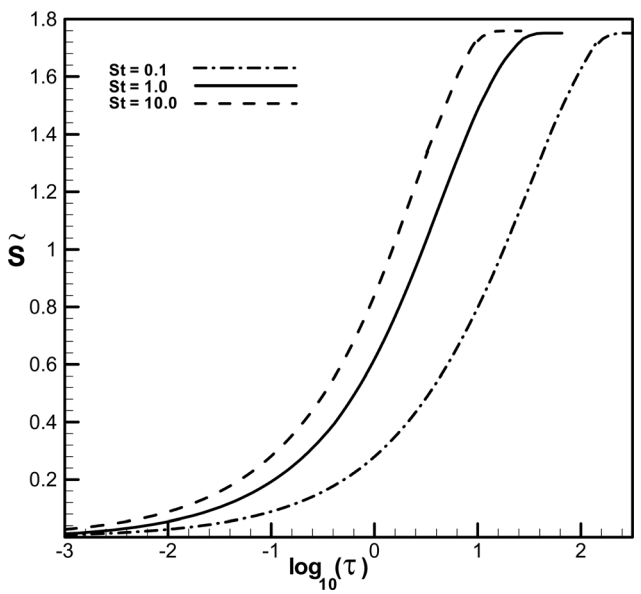

Fig. 8 Effect of the St number upon the solidification front for (Pr = 1, St = 1, $k_r = 1$, and $\alpha_r = 1$)

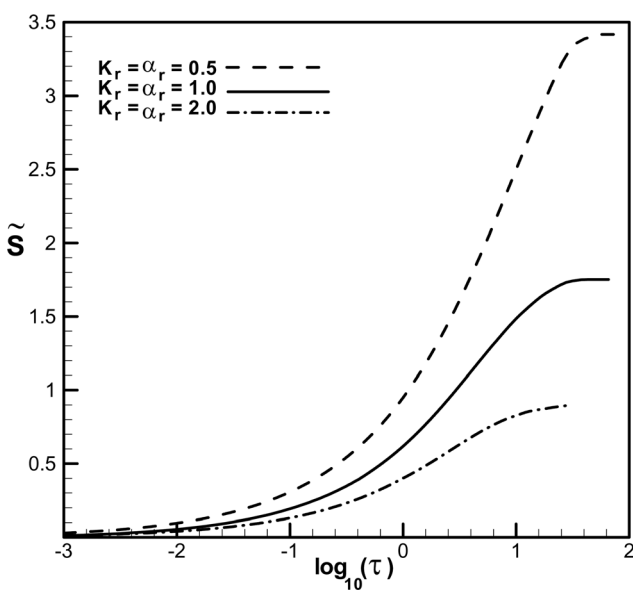

Fig. 10 Effect of the k_r and α_r variations upon the solidification front for (Pr = 1, St = 1, and $\theta_i = 1$)

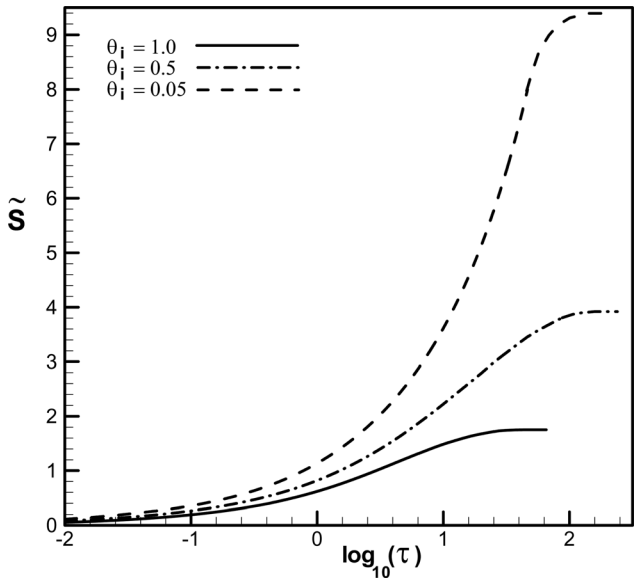

Fig. 11 Effect of the θ_i variations upon the solidification front for (Pr = 1, St = 1, $k_r = 1$, and $\alpha_r = 1$)

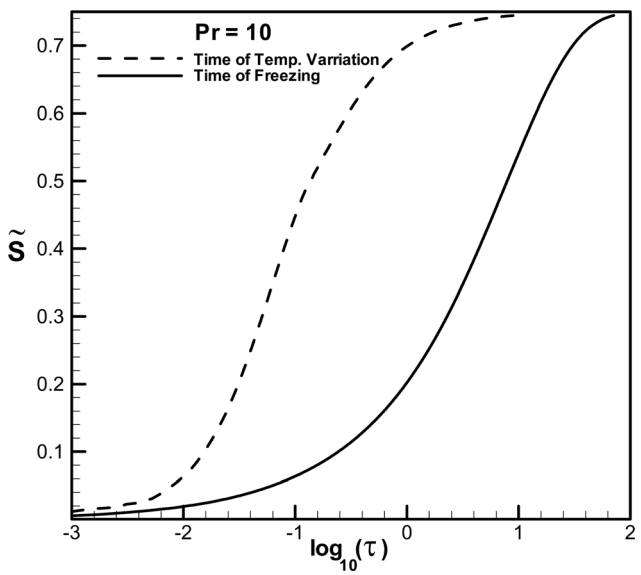

Fig. 12 Effect of the inlet temperature variations to the freeze point versus freeze time for (Pr = 10, St = 1, $k_r = 1$, $\alpha_r = 1$, and $\theta_i = 1$)

Table 1 Comparison between temperature variations and freezing time versus inlet to freeze temperature variations; time only

Total time for variation and freezing	Time for inlet to freeze temperature variations
$\log_{10}(\tau) = 1.823$ or $\tau = 66.53$	$\log_{10}(\tau) = 0.968$ or $\tau = 9.29$

the convection terms in the liquid-solid interface is negligible and the assumption of the solidification front being flat is proved by this fact; however, these convection terms will be much larger as they approach the edge of the temperature boundary layer and will affect the conduction heat transfer of the fluid, which has an important role on the termination of solidification.

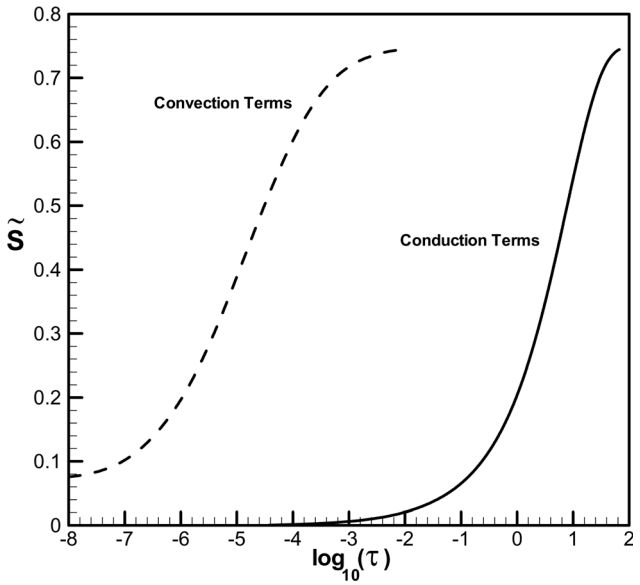

Fig. 13 Comparison of the conduction and convection terms contribution for (Pr = 10, St = 1, $k_r = 1$, $\alpha_r = 1$, and $\theta_i = 1$)

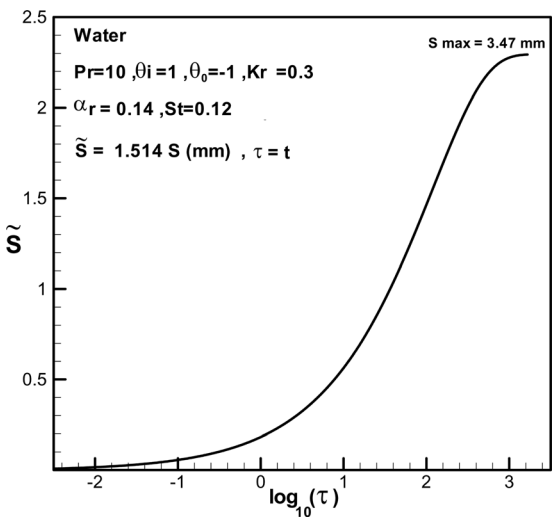

Fig. 14 Evolution of the solidification front for water with $\alpha_\circ = 1$

At last, and to complete the discussion, water solidification modeling in two-dimensional stagnation flow is considered as an example. The conditions are: $T_i = 1\,^\circ\mathrm{C}$, $T_{\text{substrate}} = -1\,^\circ\mathrm{C}$, and $a_0 = 1\,\mathrm{s}^{-1}$, along with the water properties. Figure 14 represents the results. Conversion factors are given in the legend of this figure. It is interesting to note that solidification is stopped after almost 20 min but 90% of this ultimate solidification front is formed in the first 5 min.

Here, some supplementary results are presented. Figure 15 represents the temperature profile for different times due to the solidification process and Table 2 shows the corresponding starting point of the temperature profile slope on both sides of the solid-liquid interface. This table shows that solidification is stopped just as these two slopes are equal (note that $\alpha_r = 1$). The table is presented here to show the exact numerical values of these quantities. Figure 16 provides the velocity profiles in the x direction for different times and distances from the z coordinate ($\xi = 0.3, \xi = 1.6,$ and $\xi = 3.2$). As is shown, when the solidification velocity is very high, that is, just for the initial moments, the

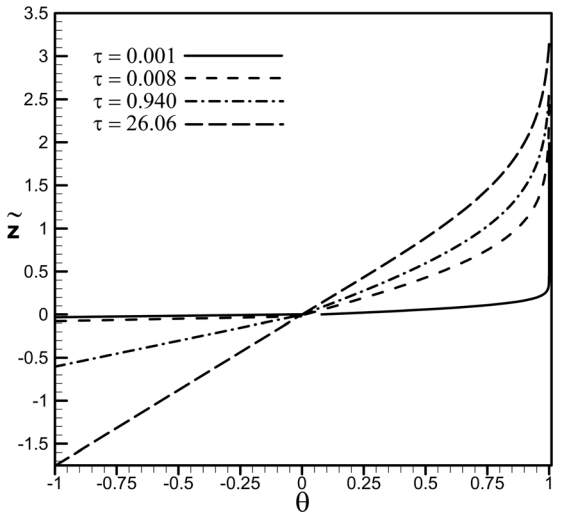

Fig. 15 Thermal profile for (Pr = 1, St = 1, $k_r = 1$, $\alpha_r = 1$, and $\theta_i = 1$)

Table 2 The temperature of the first node of the interface: lower and upper

Type of line in Fig. 4	θ_S	θ_l
Continuous line	−0.199984	0.079534
Dashed line	−0.024450	0.012544
Dotted line	−0.001599	0.000936
Long dashed line	−0.000602	0.000601

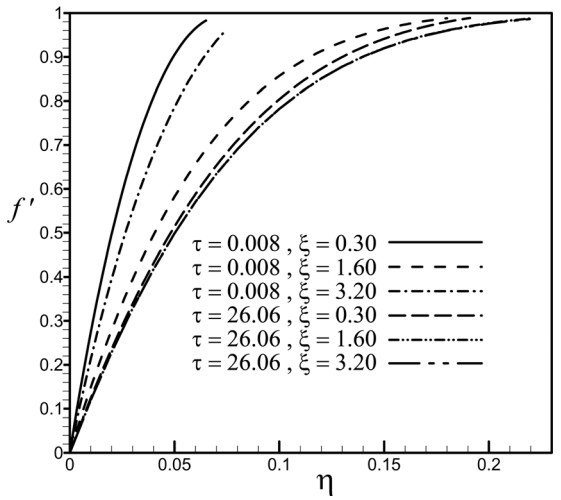

Fig. 16 Velocity profile in the *x* direction for (Pr = 1, St = 1, $k_r = 1$, $\alpha_r = 1$, and $\theta_i = 1$)

slope of the velocity profile in the boundary layer is very steep and the velocity approaches the potential flow very fast, so the thickness of the viscous boundary layer is very thin. By a gradual decrease of the solidification velocity, the unsteady case approaches the steady case of Hiemenz flow. In addition, Fig. 17 provides the velocity profile in the z-direction for different times. More complete parametric studies over the momentum equation parameters, such as pressure variation along the viscous boundary layer and shear stress have been investigated in Ref. [17] and are not repeated here.

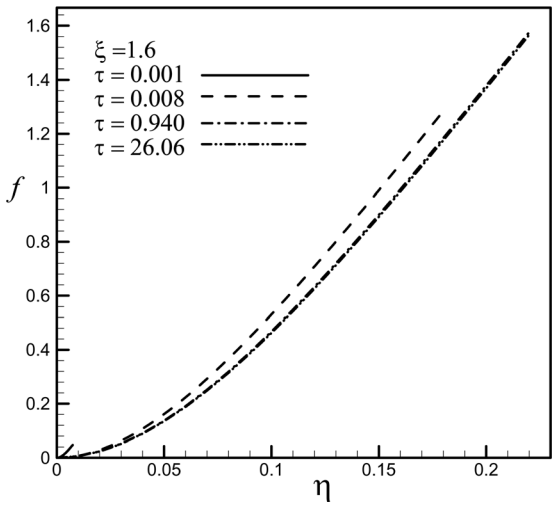

Fig. 17 Velocity profile in the *z* direction for (Pr = 1, St = 1, $k_r = 1$, $\alpha_r = 1$, and $\theta_i = 1$)

7 Conclusions

In this study, solidification has been modeled as a two-dimensional viscous stagnation-point flow on an accelerated flat plate in which pressure variations are considered along both the boundary layer and direction of flow. The solution approach has been divided into two parts: First, the exact solution for the momentum equations and, second, the numerical solution for the energy equation in the liquid phase and solid-liquid interface has been employed with which these equations have been solved at any step, simultaneously.

The results show a steady temperature boundary layer or, in more exact words, the start of the steady temperature profile slope and the ratio of the liquid to solid temperature diffusivity determine the ultimate solidification thickness, while the solidification does not stop, in theory, upon stagnant flow. It has been shown in this study that an increase of the Pr number decreases the ultimate solidification thickness and increasing k_r and/or α_r by half increases this thickness two times and vice versa. Additionally, decreasing θ_i increases this thickness while the St number variations have no effect on the ultimate solidification thickness and increasing this dimensionless number decreases the time of approach this thickness. In addition, the elimination of the temperature variations time, from the initial value to the freezing point, can produce high value of errors, such as 14% for $\mathrm{Pr} = 10$, $\mathrm{St} = k_r = \alpha_r = \theta_i = 1$ conditions, and the value of this error varies when conditions vary.

The very small effect of convection terms at the interface leads to an almost flat solidification front but these terms are very important as they are approaching the edge of the boundary layer. In fact, the solidification in stagnation flow will stop just by the existence of these terms.

Finally, a typical example of water solidification has been presented. The results provide good insight into the effect of the fluid motion on the solidification.

Nomenclature

$a(t)$ = time-dependent potential flow strain rate
$a_\circ$ = potential flow strain rate at time = 0
f = similarity function
h_{ls} = solidification latent heat
k_r = ratio of $k(k_l/k_s)$
Pe = Peclet number $(\mathrm{Pr} \cdot \mathrm{Re} = u \cdot \Delta z/\alpha_l)$
Pr = Prandtl number (ν/α_l)
$S(t)$ = solid phase thickness
$\tilde{S}$ = nondimensional solid thickness $S/\sqrt{\alpha_s/a_\circ}$

St = Stefan number $(c(T_m - T_\circ)/h_{sf})$
t = time
T = temperature
$\tilde{x}$ = nondimensional x
$\tilde{z}$ = nondimensional z

Greeks

α = coefficient of thermal diffusivity
α_l = coefficient of diffusivity of liquid
α_r = ratio of α (α_l/α_s) α_s = coefficient of thermal diffusivity of solid
ζ = variable $(z - S_{(t)})$
η = similarity variable, nondimensional z axis, $\eta = \sqrt{a_\circ/\nu}\zeta$
θ = nondimensional temperature, $(T - T_m)/(T_m - T_\circ)$
μ = viscosity
ν = kinetic viscosity
ξ = nondimensional x axis, $\xi = \sqrt{a_\circ/\nu}x$
ρ = density
τ = nondimensional time

Subscripts

i = initial temperature of fluid at potential flow
l = liquid
s = solid
m = melting point
o = at time = 0

References

[1] Stefan, J., 1891, "Uber die theorie der eisbildung, insbesondere uber die eisbildung in polarmaere," Ann. Phys. Chem., **42**, pp. 269–286.
[2] Goodrich, L. E., 1978, "Efficient Numerical Technique for One-Dimensional Thermal Problems With Phase Change," Int. J. Heat Mass Transfer, **21**, pp. 615–621.
[3] Sparrow, E. M., Ramsey, J. W., and Harris, S., 1981, "The Transition From Natural Convection Controlled Freezing to Conduction Controlled Freezing," ASME J. Heat Transfer, **103**, pp. 7–13.
[4] Lacroix, M., 1989, "Computation of Heat Transfer During Melting of a Pure Substance From an Isothermal Wall," Numer. Heat Transfer, Part B **15**, pp. 191–210.
[5] Yeoh, G. H., Behnia, M., De Vahl Davis, G., and Leonardi, E., 1990, "A Numerical Study of Three-Dimensional Natural Convection During Freezing of Water," Int. J. Numer.Methods Eng., **30**, pp. 899–914.
[6] Hadji, L. and Schell, M., 1990, "Interfacial Pattern Formation in the Presence of Solidification and Thermal Convection," Phys. Rev. A, **41**, pp. 863–873.
[7] Hanumanth, G. S., 1990, "Solidification in the Presence of Natural Convection," Int. Commun. Heat Mass Transfer, **17**, pp. 283–292.
[8] Oldenburg, C. M., and Spera, F. J., 1992, "Hybrid Model for Solidification and Convection," Numer, Heat Transfer, Part B, **21**, pp. 217–229.
[9] Trapaga, G., Matthys, E. F., Valecia, J. J., and Szekely, J., 1992, "Fluid Flow, Heat Transfer and Solidification of Molten Metal Droplets Impinging on Substrates: Comparison of Numerical and Experimental Results," Metall. Trans. B, **23B**, pp. 701–718.
[10] Watanabe, T., Kuribayashi, I., Honda, T., and Kanzawa, A., 1992, "Deformation and Solidification of a Droplet on a Cold Substrate," Cham. Eng. Sci., **47**, pp. 3059–3065.
[11] San Marchi, C., Liu, H., Lavernia, E. J., and Rangel, R. H., 1993, "Numerical Analysis of the Deformation and Solidification of a Single Droplet Impinging on to a Flat Substrate," J. Mater. Sci., **28**, pp. 3313–3321.
[12] Brattkus, K., and Davis, S. H., 1988, "Flow Induced Morphological Instabilities: Stagnation-Point Flows," J. Cryst. Growth, **89**, pp. 423–427.
[13] Rangel, R. H., and Bian, X., 1994, "The Inviscid Stagnation-Flow Solidification Problem," Int. J. Heat Mass Transfer, **39**(8), pp. 1591–1602.
[14] Lambert, R. A., and Rangel, R. H., 2003, "Solidification of a Super-Cooled Liquid in Stagnation-Point Flow," Int. J. Heat Mass Transfer, **46**, pp. 4013–4021.
[15] Rangel, R. H., and Bian, X., 1996, "The Viscous Stagnation-Flow Solidification Problem," Int. J. Heat Mass Transfer, **39**(17), pp. 3581–3594.
[16] Yoo, J. S., 2000, "Effect of Viscous Plane Stagnation Flow on the Freezing of Fluid," Int. J. Heat Fluid Flow, **21**, pp. 735–739.
[17] Shokrgozar Abbasi, A., and Rahimi, A. B., 2012, "Investigation of Two-Dimensional Unsteady Stagnation Flow and Heat Transfer Impinging on an Accelerated Flat Plate," ASME J. Heat Transfer, **134**(6), p. 064501.
[18] Hong, C., Yamamoto, T., Asako, Y., and Suzuki, K., 2012, "Heat Transfer Characteristics of Compressible Laminar Flow Through Microtubes," ASME J. Heat Transfer, **134**, p. 011602.
[19] Alassar, R., and Abushoshah, M., 2012, "Hagen-Poiseuille Flow in Semi-Elliptic Microchannels," ASME J. Fluids Eng., **134**, p. 124502.
[20] Norouzi, M., Rezaei Niya, S. M., Kayhani, M. H., Shariati, M., Karimi Demneh, M., and Naghavi, M. S., 2012, "Exact Solution of Unsteady Convective Heat Transfer in Cylindrical Composite Laminates," ASME J. Heat Transfer, **134**, p. 101301.
[21] Pitts, D. R., and Sissom, L. E., 1977, *Theory and Problems of Heat Transfer*, Schaum's Outlines Series, McGraw-Hill, New York.